Switchable circular-to-point converter based on holographic polymer-dispersed liquid-crystal technology

Hailiang Zhang, Haiqing Xianyu, Jianhua Liang, Yan Bétrémieux, Gregory P. Crawford, John Noto, and Robert Kerr

We demonstrate the use of a switchable circular-to-point converter (SCPC) device based on holographic polymer-dispersed liquid-crystal technology for application in lidar detection and optical telecommunication. A SCPC device converts the Fabry–Perot ring pattern into a single point or an array of points, while an external electrical field on the SCPC deactivates the conversion. Stacking different SCPC elements gives a random optical switch for applications in lidar detection and optical telecommunication. Two types of SCPC designs are analyzed and one is chosen and built for testing.

OCIS codes: 090.2890, 050.7330.

1. Introduction

Fabry–Perot interferometers are widely used in lidar detection of atmospheric, environmental, and climatic changes,[1,2] as well as in optical telecommunication,[3] because of their high resolution and high throughput. In some cases, the total throughput of a Fabry–Perot interferometer is the only concern. However, in others, the spectral distribution of light is of great interest. Traditionally, it has been difficult to collect the spectral information distributed in its circular interference pattern. Recently, a holographic optical element was developed for transforming a circular Fabry–Perot fringe pattern into a series of point images.[4,5] Although this HOE device is revolutionary, it requires multiple detectors to collect the different spectral channels that are distributed in the fringe pattern and lacks a dynamic switchable function that is important in many applications.

We propose a switchable circular-to-point converter (SCPC) based on holographic polymer-dispersed liquid-crystal (HPDLC) technology.[6,7] A SCPC device converts the Fabry–Perot ring pattern into a single point or an array of points without applied voltage, while an external electric field applied to the SCPC will deactivate the conversion. Figure 1 illustrates a system using a SCPC device. The input signal is spectrally discriminated through the Fabry–Perot etalon into a circular fringe pattern; a SCPC converts the collimated, circularly distributed signal into a focusing point when no external field is applied to the SCPC. When an external electric field above a threshold value is applied to the SCPC, the SCPC becomes transparent and lets the signal pass through. Moreover, a SCPC is designed with a ring pixel pattern identical to the fringe pattern of the Fabry–Perot interferometer and each pixel can be independently electrically switched. Thus the multiple-channel SCPC is able to collect the signal of different wavelength channels that are discriminated by the Fabry–Perot interferometer.

2. Principle and Modeling of a Switchable Circular-to-Point Converter

The SCPC is based on HPDLC technology, which is widely applied within the reflective flat panel display industry, and is now applicable to optical switching and wavelength-division-multiplexing devices in fiber-optic communication. HPDLCs are descendant of the polymer-dispersed liquid crystal (LC) developed by Doane and co-workers[6–8] in the mid-1980s. A LC monomer solution undergoes a photoinduced phase separation initiated by interfering laser beams, resulting in LC droplets encapsulated in a rigid polymer binder that are spatially segregated throughout the sample.

H. Zhang (zhang@sci-sol.com), Y. Bétrémieux, J. Noto, and R. Kerr are with Scientific Solutions, Inc., 55 Middlesex Street, North Chelmsford, Massachusetts 01863-1561, USA. H. Xianyu, J. Liang, and G. P. Crawford are with the Department of Physics, Brown University, Providence, Rhode Island 02912, USA.

Received 7 July 2006; accepted 2 October 2006; posted 13 October 2006 (Doc. ID 72784); published 21 December 2006.

0003-6935/07/020161-06$15.00/0

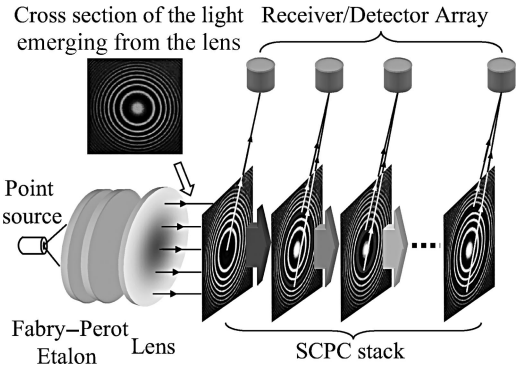

Fig. 1. SCPC converts the collimated circularly distributed signal into a focusing point.

Fabrication begins with a miscible mixture of LC and prepolymer that is subsequently exposed to the interference pattern of two laser beams, operating in the visible or ultraviolet depending on the choice of prepolymer. The result is a periodic array of planes alternately rich in LC droplets and polymer, as shown in Fig. 2.

The interference fringe spacing (Λ) of the grating is well described by the grating equation: $\Lambda = \lambda/(2n|\sin\alpha|)$, where λ is the wavelength of light, n is the average index of the mixture before polymerization, and α is half the angle between the two exposing beams. During formation, the monomer diffuses to the high-intensity regions of the interference pattern as polymerization forces the LC to the low-intensity regions, a process subsequently followed by phase separation into droplets. These LC droplets are governed by surface-anchoring conditions and polymer morphology and usually result in bipolar configurations with an axial symmetry. When materials are chosen such that a net index of refraction mismatch exists between the LC droplet layers and the polymer binder, strong Bragg reflection will occur. However, when a sufficient electric field is applied to reorient the LC droplets, the refractive index of the LC may match that of the polymer (n_p), inducing a transparency of the HPDLC. Fabrication of a SCPC is similar to the fabrication of a traditional HPDLC, except, to create the expected focusing effect of the SCPC, one of the two holographic-writing beams should be a plane wave and the other should be a spherical wave.

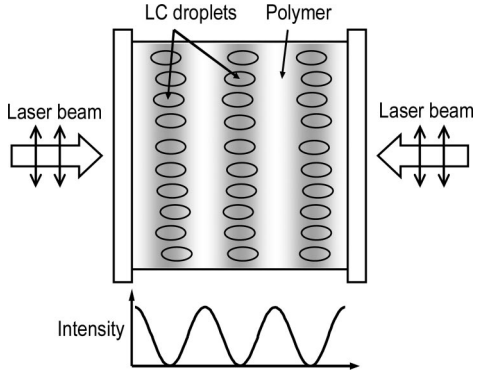

Fig. 2. LC droplets inside the polymer network of a HPDLC sample.

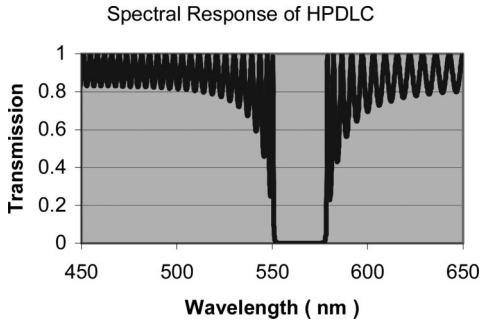

Fig. 3. Simulation of the spectral response of normally incident light passing alternating layers of liquid crystal and polymer.

The SCPC is used in tandem with a Fabry–Perot etalon that disperses the different wavelength channels into a circular fringe pattern. The Fabry–Perot etalon is comprised of two optical glasses with high-reflection coatings; when light passes through the etalon, the interference arising from the multireflections will allow certain wavelengths to pass through and reflect the other wavelengths. When the incident light is not collimated, the intensity of light $I(\theta, \lambda)$ coming through an ideal Fabry–Perot etalon (one with no defects) is given by

$$I(\theta,\ \lambda) = I_0(\lambda)/\left[1 + (2F/\pi)^2 \sin^2(\delta/2)\right], \qquad (1)$$

with $\delta = 4\pi nd\cos(\theta)/\lambda$, where λ is the wavelength of light, $I_0(\lambda)$ is the intensity of incident light in the center of each of the Hadinger fringes, d is the plate separation, n is the index of refraction of the material between the etalon plates, and F is the finesse of the etalon. When the light source is monochromatic, the Fabry–Perot system allows transmission of light at only specific incidence angles. When the light source has a spectral distribution, the fringe pattern will separate the wavelengths of the signal.

To decide the working spectral range of a SCPC, we treat the HPDLC microstructure as alternating layers of liquid crystal and polymer and simulate the spectral response of the SCPC. Figure 3 is a model of the spectral response simulating normally incident polarized light passing alternating layers of liquid crystal

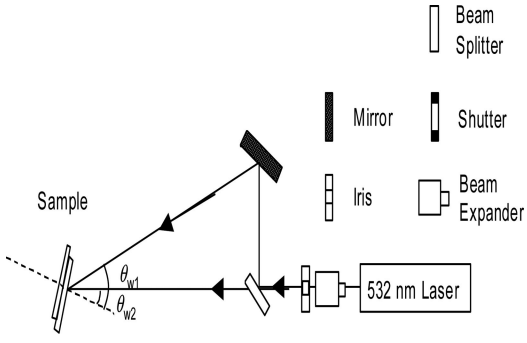

Fig. 4. Optical setup for fabrication of SCPC.

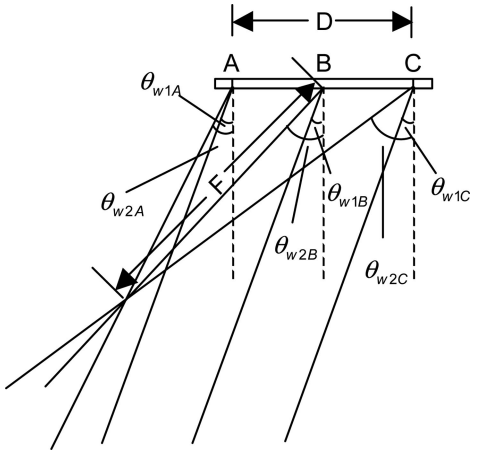

Fig. 5. Recording beam configuration near the SCPC sample.

and polymer, using Berreman's 4-by-4 method.[9] The polarization direction of light is assumed to be along the director direction of liquid crystals. In the model the refractive indices of the liquid crystal and polymer were 1.56 and 1.487, respectively. The thickness of both the liquid-crystal layers and the polymer layers was 91.4 nm.

3. Optical Design for a Switchable Circular-to-Point Converter

Two types of SCPC unit are designed in the 1.5 μm range for optical telecommunication applications. In the first device, the HPDLC can focus the collimated incident light to a point. In the second type of SCPC, the HPDLC is a traditional transmission HPDLC whose function is to steer the beam; a lens between the SCPC and the detector focuses the steered diffracted beam. The holographic setup for the second type of SCPC is illustrated in Fig. 4.

In the first type of SCPC device, the HPDLC is designed similar to a holographic lens.[10] To fabricate The HPDLC for the first type of SCPC, an interference pattern is constructed using a point source and a plane wave. The point source is generated by a lens with a focal length of F in the optical path of one recording beam, and the lens is placed at a distance $2F$ from the sample cell. The HPDLC is recorded using a 532 nm laser, while the operational wavelength is 1540 nm for optical communication applications. One challenge resulting from the difference in the recording and reading wavelengths is that the diffracted beam is astigmatic and the diffraction efficiency is not homogeneous when reading with the 1540 nm laser. The recording and reading optics of the HPDLC across the center of the HPDLC area have been simulated. The reading beam wavelength is chosen to be 1540 nm. The recording beam configuration near the sample is illustrated in Fig. 5. In the model, the diffraction angle at the center of the HPDLC is designed to be $\theta = 79°$. Assuming the refractive index of the medium for the wavelength of the laser is identical for both the read and write beams, or $n_w = n_r = 1.5$, the incident angles of recording beams at the center of the HPDLC can be derived using Bragg's law: $\theta_{w1} = 43°59'$ and $\theta_{w2} = 20°51'$. The diameter of the effective HPDLC area is $D = 2.54$ mm.

For the collimated recording beam, the incident angle is identical on different locations of the HPDLC: $\theta_{w2A} = \theta_{w2B} = \theta_{w2C} = 20°51'$. The incident angles of the diverging recording beam at different locations are calculated for a series of F. With the incident angles of the recording beams determined, the Bragg-matched incident angle and diffraction angles for the 1540 nm reading beam on a series of locations across the HPDLC area along the line AC is calculated. The normal incidence deviates from the Bragg-matched incidence when the incident location is moving away from the center, B. The Bragg-matched incident angles and diffraction angles at A and C are listed in Table 1, which shows the largest deviations from normal incidence. Considering the angular dependence of the diffraction efficiency, this result indicates the diffraction efficiency decreases with an increase in the distance from the incident spot to the center of the HPDLC for normal incident reading at 1540 nm. The deviation of Bragg-matched incidence from normal incidence decreased with increasing F. The diffraction angles for normal incident reading at 1540 nm are also calculated. These angles are different from the Bragg-matched diffraction angles. The diffraction angles at A and B are included in Table 1. It is important to notice that when F is less than 1000 mm, the diffraction beam at the left edge, A, will be completely reflected at the glass–air interface and trapped in the HPDLC until finally escaping from the edge. This total internal reflection (TIR) further decreases the diffraction efficiency at the edge of the HPDLC area.[11] To avoid the TIR effect, the focal length of the lens should be greater than 1000 mm. When the dif-

Table 1. Incident Angles of the Diverging Recording Beam at Different Locations

F (mm)	θ_{w2A} (°)	θ_{w2C} (°)	θ_{rbA} (°)	θ_{dbA} (°)	θ_{rbC} (°)	θ_{dbC} (°)	θ_{dnA} (°)	θ_{dnC} (°)	d (mm)
900	44.17	43	−0.49	TIR	0.449	75.6	74.14	TIR	N/A
1000	44.11	43.06	−0.44	83.21	0.449	75.91	87.12	74.57	4.801
1100	44.07	43.11	−0.40	82.73	0.407	76.17	85.71	74.92	4.801
1200	44.03	43.15	−0.37	82.36	0.373	76.38	84.83	75.22	4.801
1300	43.99	43.18	−0.34	82.05	0.344	76.57	84.18	75.48	4.801
1500	43.49	43.24	−0.29	81.59	0.298	76.87	83.26	75.91	4.801
1700	43.9	43.28	−0.26	81.25	0.263	77.11	82.64	76.24	4.831

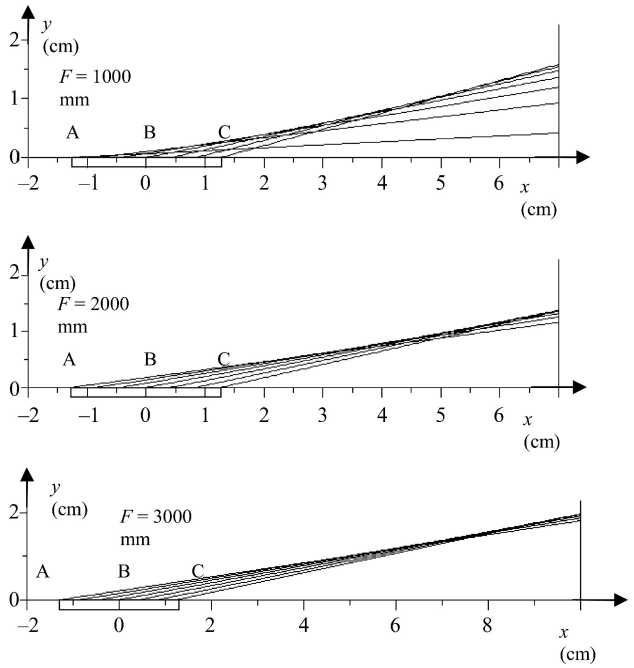

Fig. 6. Diffracted beam profiles of the 2.54 cm (1 in.) HPDLC. The focal lengths of the cylindrical lens for fabrication are 1000, 2000, and 3000 mm from top to bottom.

fraction angles are known, the converging properties of the diffracted beam in the x–y plane can be derived from Bragg's law. Figure 6 shows the convergence properties of the diffracted beams across the center of the cell in the y direction. The focus is not ideal in the x–y plane. Increasing F, the waist of the diffracted beam (the thinnest width of the diffracted beam) decreases, and the position of the beam waist moves away from the HPDLC. To obtain relatively good focus, a lens with a large focal length is preferred in the recording optics. Since the lens is placed $2F$ from the HPDLC during exposure, a large F brings inconvenience to the fabrication process.

In the simulation above, only the locations across the center of the HPDLC area are considered. A qualitative simulation of various locations over the entire HPDLC area using ZEMAX, an optical simulation and design software, revealed the focusing of the diffracted beam is also astigmatic. The convergence of the diffracted beam in the x–y plane is sharper than that in the z direction. Therefore the linear dimension of the focus point is larger than that of the beam waist calculated in the simulation. The large difference between the recording and reading wavelength of the 32-channel SCPC devices results in a substantial astigmatism in the diffracted light. Our investigation also reveals that the ideal focus of the diffracted beam could not be realized employing simply configured recording beams (collimated, converging, diverging, etc.) when the recording and reading wavelengths are different. Therefore the SCPC with built-in focus is not an appropriate choice for 32-channel SCPC devices, which operate in the near-infrared region of the spectrum (~1500 nm). A decision was made to fabricate only the second type of SCPC, which merely redirects incident light, and an external lens is used to focus the diffracted beam.

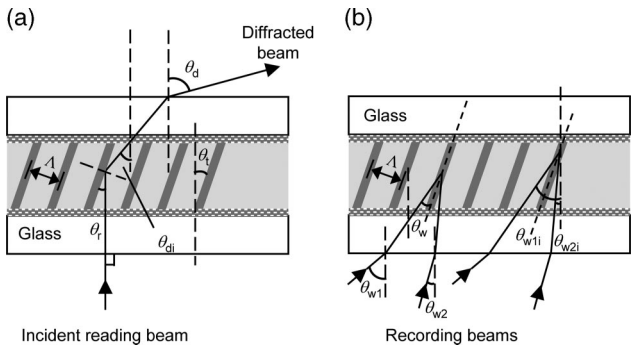

Fig. 7. (a) Reading beam configuration and (b) recording beam configuration of the beam steering HPDLC for SCPC.

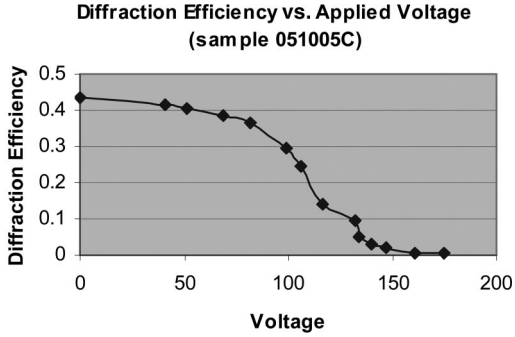

Fig. 8. Electro-optical response curve of a SCPC.

4. Experimental Result

The SCPC units are fabricated with patterned indium tin oxide glass substrates. The holographic recording setup for fabricating the SCPC units is illustrated in Fig. 4. The recording beam and the reading beam configurations are shown in Fig. 7, the two recording beam incident angles are $\theta_{w1} = 41°25'$ and $\theta_{w2} = 18°25'$. The cell gap was controlled by 15 μm fiber spacers. The cells are balloon pressed for 12 min under a pressure of 4.5 psi (or 31,026 Pa) to ensure cell gap homogeneity before the holographic exposure. The exposure time is 5 min and the total output power of the laser is set at 3 W during the exposure. After exposure, the cell is postcured in a 3 W laser beam to polymerize the monomers outside the HPDLC area. The edges of the

Table 2. List of the Switching Voltage, Diffraction Efficiency, and Contrast Ratio of Five SCPC Devices

Sample Number	Switching Voltage (V)	Diffraction Efficiency (%)	Contrast Ratio
051005C	174.7	43.40	90.7
050605D	129	40.60	57.5
051005E	200	34.50	42.5
051005B	196	33.50	22.4
051005D	152	29.50	26.5

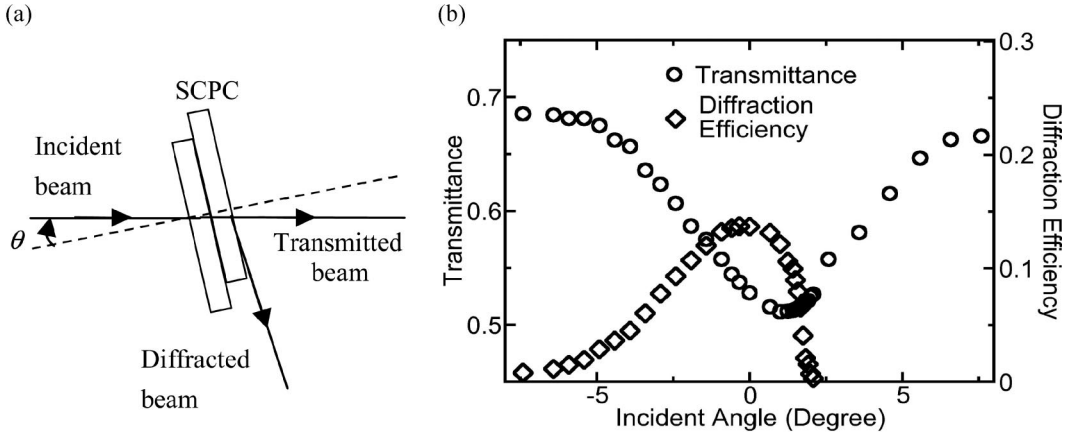

Fig. 9. (a) Definition of the reading beam incident angle θ in the angular dependence measurement. (b) Transmittance and diffraction efficiency as a function of the incident angle of the SCPC units at a wavelength of 1540 nm.

cells are secured with 5 min epoxy. The prepolymerization mixture consists of 43.36% of the liquid crystal BL038; 35.92% of the monomer dipentaerythritol pentaacrylate (DPHA); 10.27% of the monofunctional monomer vinyl neononanoate (VN); and 10.45% of a mixture of a photoinitiator consisting of Rose Bengal (photoinitiator), N-phenylglycine (NPG, co-initiator), and 1-vinyl-2-pyrrolidinone (NVP, solvent and chain terminator) with the weight ratios of 4%, 10%, and 96%, respectively. The five pieces of the SCPC devices are fabricated and tested. A standard electro-optical response curve of a SCPC is shown in Fig. 8, the switching voltage may vary for different SCPC devices. Diffraction efficiency is defined as the ratio of the diffracted light intensity to the input light intensity when there is no applied voltage. Switching voltage is defined as the minimum voltage to fully switch the SCPC. As shown in Fig. 8, the switching voltage of the device 051005C is 174.7 V. Table 2 lists the switching voltage and diffraction efficiency of the five SCPC devices. The contrast ratio of a SCPC device is defined as the ratio of the diffraction efficiency without an applied voltage to that under the switching voltage. As a function of optical switching, the contrast ratio is a direct description of the signal-to-noise ratio when the diffracted light beam is collected as the signal.

The dependence of transmittance and diffraction efficiency as a function of the incident angle of the reading beam is characterized to evaluate the holographic recording optical setup. A 1540 nm fiber laser generates the incident beam. The transmitted beam intensity and diffracted beam intensity are measured using a Melles Griot universal powermeter and an OPHIR infrared powermeter with various reading beam incident angles that are defined in Fig. 9(a). The reading beam incident angle is positive in Fig. 9(a). The zero field transmittance and diffraction efficiency as a function of incident angles are presented in Fig. 9(b). The diffraction efficiency approached a maximum value at normal incidence, while the transmittance is minimized when the incident angle is 1°. This result proves that the choice and control of recording beam incident angle is optimized for normal incidence reading of the designed wavelength. When the reading beam incident angle is greater than 1°, the diffraction efficiency decreases much faster than the increase of the transmittance. The abruptness of the decrease in diffraction efficiency is due to the increase of the diffraction angle. The diffraction angle increased with an increase of the incident angle. The designed diffraction angle in the device is 79° in air and the diffraction angle inside the SCPC is close to the TIR angle at the glass–air interface. The efficiency of the antireflection coating on the glass substrates decreased substantially when the diffraction angle was close to the TIR angle and the diffracted light would be totally reflected when the TIR angle was reached or exceeded. Conversely, the performance of the antireflection coating hardly changed for the transmitted light. The change in transmittance with angle can be mostly attributed to the change of diffraction efficiency with the change of incident angle. Therefore, the transmission data used to fit diffraction efficiency for transmission gratings is derived using coupled-wave theory[12,13]:

$$\eta = \{k^2/[k^2 + (\Delta\alpha/2)^2]\} \sin\{kL[1 + (\Delta\alpha/2k)^2]^{1/2}\}, \quad (2)$$

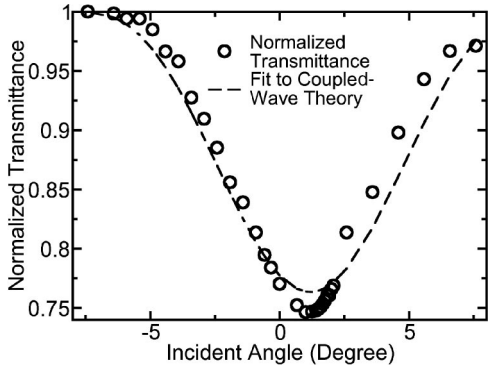

Fig. 10. Normalized transmittance is fit to the formula for a transmission grating derived using coupled-wave theory.

where $k = \pi n_1 \cos(2\theta_B)/\lambda \cos \theta_B$ is the coupling constant, and $\Delta\alpha = -4\pi n_0 \Delta\theta \sin \theta_B/\lambda$ is the phase mismatch. Here λ is the reading beam wavelength, θ_B is the Bragg angle, n_0 is the average refractive index of the HPDLC, n_1 is the index modulation of the grating, and $\Delta\theta$ is the deviation from the Bragg angle. The corresponding transmittance is given by $1 - \eta$, provided that all other losses are neglected.

This measurement is for *p*-polarized light only; therefore, the coupling constant k is calculated for *p*-polarized light and the fitting is only valid for *p*-polarized light. The best-fit curve is presented in Fig. 10. The index modulation of the HPDLC is $n_1 = 0.02 \pm 0.002$.

5. Discussion

So far all of the SCPC and HPDLC samples we have prepared have strong polarization dependence; the light of *p* polarization has high diffraction efficiency, whereas the light of *s* polarization has very low diffraction efficiency. Also in our samples we noticed the light scattering that decreased the transmission. We are going to probe these in our future research and hope to get a polarization-independent SCPC device. We hypothesize the cause of the polarization dependence is that the liquid-crystal droplets have no symmetry for the *s*-polarization direction and the *p*-polarization direction.

6. Conclusions

A switchable circular-to-point converter based on holographic polymer-dispersed liquid-crystal technology has been demonstrated as a device with applications in optical telecommunication and lidar detection. The switchable function allows the easy detection of signals from a Fabry–Perot interferometer. Two types of SCPC were investigated and the astigmatism in the diffracted light of the first type of SCPC with built-in focus was revealed when the recording and reading sources had different wavelengths. The second type of SCPC was fabricated and high diffraction efficiency of up to 43% was demonstrated.

This research was supported by the NASA Goddard Space Flight Center Small Business Innovative Research (SBIR) program under contract number NAS5-02117 and the Missile Defense Agency SBIR under contract number F33615-03-C-4101.

References

1. R. B. Kerr, J. Noto, R. S. Lancaster, M. Franco, R. J. Rudy, R. Williams, and J. H. Hecht, "First Fabry–Perot observations of He (2^3P) 10830 Å emission at Millstone," Geophys. Res. Lett. **23,** 3239–3242 (1996).
2. J. Noto, K. E. Schneller, W. J. Schneller, R. B. Kerr, and R. A. Doe, "Nematic Fabry–Perot etalons for ground and space based atmospheric remote sensing," in Proc. SPIE **3118,** 368–377 (1997).
3. H. Zhang, Y. Betremieux, J. Noto, and R. B. Kerr, "Novel tunable liquid crystal Fabry–Perot filters for fiber optical system," in Proc. SPIE **4383,** 64–72 (2001).
4. M. J. McGill, M. Marzouk, V. S. Scott III, and J. D. Spinhirne, "Holographic circle-to-point converter with particular applications for LIDAR work," Opt. Eng. **36,** 2171–2175 (1997).
5. M. McGill and R. Rallison, "Holographic optics convert rings to points for detection," Laser Focus World **37,** 131–136 (2001).
6. G. P. Crawford and S. Zumer, *Liquid Crystals in Complex Geometry* (Taylor and Francis, 1996).
7. G. P. Crawford and J. W. Doane, "Polymer dispersed liquid crystals," Condens. Matter News **1,** 5–11 (1992).
8. J. W. Doane, *Liquid Crystals—Application and Uses* (World Scientific, 1990), Vol. 1, Chap. 14.
9. D. W. Berreman, "Optics in stratified and anisotropic media: 4×4-matrix formulation," J. Opt. Soc. Am. **62,** 502–510 (1972).
10. A. K. Richter and F. P. Carlson, "Holographically generated lens," Appl. Opt. **13,** 2924–2930 (1974).
11. H. Xianyu, J. Qi, R. F. Cohn, and G. P. Crawford, "Total-internal-reflection mode in holographic polymer dispersed liquid crystals," Opt. Lett. **28,** 792–794 (2003).
12. P. Yeh and C. Gu, *Optics of Liquid Crystals* (Wiley, 1999).
13. H. Kogelnik, "Coupled wave theory for thick hologram gratings," Bell Syst. Tech. J. **48,** 2909–2947 (1969).